



High-resolution aerosol retrieval over urban areas using sentinel-2 data

Yue Yang^a, Yunping Chen^{a,*}, Kangzhuo Yang^a, Jan Cermak^{b,c}, Yan Chen^a

^a School of Automation Engineering, University of Electronic Science and Technology of China, Sichuan, Chengdu 611731, China

^b Institute of Meteorology and Climate Research, Karlsruhe Institute of Technology (KIT), Karlsruhe 76131, Germany

^c Institute of Photogrammetry and Remote Sensing, Karlsruhe Institute of Technology (KIT), Karlsruhe 76131, Germany



ARTICLE INFO

Keywords:
Aerosol retrieval
Urban areas
Sentinel-2
High resolution

ABSTRACT

Accurate retrieval of Aerosol Optical Depth (AOD) data from satellite remote sensing images over urban areas is of great importance, e.g. for air-quality monitoring. However, limited by coarse spatial resolution, available aerosol products are unable to fulfil the increasing demand of aerosol retrieval below the city scale. To address this issue, a new high-resolution (60 m) aerosol retrieval algorithm based on Sentinel-2 data over urban areas was developed. To improve the estimation of surface reflectance, two algorithms: (1) the new visible/2.19 μm surface reflectance relationships as a function of normalized difference vegetation index (NDVI) for vegetated areas; and (2) the surface reflectance database preconstructed from the operational high-quality and high-resolution Landsat 8 surface reflectance products for bright areas, were adopted depending on the surface types. For validation, the derived retrievals from Sentinel-2, along with the operational MODerate resolution Imaging Spectrometer Collection 6 (C6) aerosol products (MOD04_L2 and MCD19A2), were compared with measurements from Aerosol Robotic Network (AERONET) stations. The validation results show that the Sentinel-2 AOD retrievals agreed well with the AERONET AOD measurements, with an overall correlation coefficient of 0.907, expected error (EE) of 73.76%, mean absolute error (MAE) of 0.087, and root mean square error (RMSE) of 0.117. Comparison of the results with MOD04_L2 products (10 km) show that the Sentinel-2 AODs were superior in the situations considered, indicating that the new algorithm performed better in AOD retrieval over urban areas. Compared with the fine spatial resolution MCD19A2 products (1 km), retrievals of the proposed algorithm were comparable. The new algorithm is able to retrieve high-resolution AODs reasonably well from Sentinel-2 images over urban areas, and can provide continuous and detailed aerosol spatial distributions. Owing to the ability of the Sentinel-2 satellite to provide observations at 5-day intervals, the proposed algorithm is capable of monitoring aerosol distributions at relatively fine temporal resolution.

1. Introduction

Atmospheric aerosols, including those from natural and anthropogenic sources, play an important role in the climate system and environmental pollution. In the climate system, aerosols not only affect the radiative energy balance by interacting with solar and terrestrial radiation but also change cloud properties and lifetimes (Hsu et al., 2013). Environmentally, aerosols are known as the main cause of air pollution with significant negative effects on human health (Kaufman et al., 2002; Li et al., 2011; Ramanathan et al., 2001). Therefore, developing approaches to retrieve aerosol properties and fully understand the impact of aerosol particles is of great importance.

Currently, remote sensing technology, with the advantages of timeliness, periodicity, and large scales, has been an effective method for

detecting the optical properties and spatial distribution of aerosols (Wei et al., 2017). The spectral aerosol optical depth (AOD) is an effective quantitative parameter to estimate the total aerosol amount in the atmosphere (Clarke et al., 2001; Holben et al., 2001). Over the past 40 years, considerable efforts have been made to retrieve AOD from satellite remote sensing images, as well as its regional and temporal patterns. For example, investigations have focused on retrieving AOD from the surface reflectance relationships between the visible (VIS) and 2.1 μm channels (Gupta et al., 2016; Kaufman et al., 1997b; Levy et al., 2007b), precalculated surface reflectance databases (Hsu et al., 2013; Luo et al., 2015), temporal signatures (Liang et al., 2006), the blurring effect (Tanre et al., 1988), multiangular information (Diner et al., 2005; North, 2002), and polarization information (Deuze et al., 2001). The famous MODerate resolution Imaging Spectroradiometer (MODIS) Dark Target

* Corresponding author.

E-mail address: chenyp@uestc.edu.cn (Y. Chen).

(DT) algorithm is a widely used aerosol retrieval algorithm (Kaufman et al., 1997b; Levy et al., 2007b). With empirical VIS/2.1 μm surface reflectance relationships, DT successfully retrieved AODs from the MODIS measurements. However, suitability only for vegetated surfaces, the DT method performs negatively for bright surfaces and has been validated to have a positive bias when applied to urban areas (Gupta et al., 2016; Munchak et al., 2013). As an alternative algorithm, the Deep Blue (DB) algorithm was developed for retrieving aerosol properties over bright surfaces (Hsu et al., 2006). Furthermore, as an improvement, the enhanced DB algorithm has been developed for obtaining aerosol information over the entire cloud-free and snow-free land surfaces (Hsu et al., 2013). The DT algorithm, together with the enhanced DB algorithm have been used for producing the MODIS Level-2 aerosol products by National Aeronautics and Space Administration (NASA).

Currently, with worsening urban pollution, the retrieval of aerosol properties over urban areas has become increasingly needed to better understand spatial patterns, and as a basis for urban planning (Huang et al., 2014; Tang et al., 2016). However, developed for MODIS, neither the DT algorithm nor the DB algorithm cannot easily be used to monitor atmospheric aerosols within a city. To solve this problem, some research have focused on high-resolution aerosol retrieval from the MODIS measurements. For examples, the simplified high resolution MODIS aerosol retrieval algorithm (SARA) and the regionally robust high-spatial-resolution aerosol retrieval algorithm retrieved 500 m and 1 km AODs from MODIS measurements, respectively (Bilal et al., 2013; Wei et al., 2019b). Recently, the Landsat series satellites, for their long-term data records at outstanding 30 m resolution every 16 days have been popular for obtaining high-resolution AOD information. The simple, universal and high-resolution Landsat (SUHL) algorithm combining the top of atmosphere (TOA) reflectance at shortwave infrared (SWIR) channel and Landsat 4–7 surface reflectance climate data records retrieved 30 m AODs from Landsat series images (Wei et al., 2017). The improved aerosol retrieval algorithm for Landsat Enhanced Thematic Mapper Plus (ETM+) images (ImAero-Landsat), as an improvement of the SARA, also retrieved 30 m retrievals from Landsat ETM+ measurements (Luo et al., 2015).

Sentinel-2 is a mission of European satellites designed to deliver land remote sensing data. Consisting of twin polar-orbiting satellites, Sentinel-2A and Sentinel-2B, Sentinel-2 provides high spatial resolution observations (10 m, 20 m, and 60 m) at relative high revisit time (5 days with 2 satellites, and 2–3 days at mid-latitudes). Comparing with its contemporaries, such as MODIS, Landsat Thematic Mapper (TM), Landsat ETM+, and Landsat 8, Sentinel-2 is superior for characterizing high spatial resolution and relatively high temporal resolution simultaneously, leading to the possibility of retrieving aerosol properties at high spatial resolution and fine temporal resolution. However, because of the differences in spectral response functions and spectral channels among different sensors, the algorithms described above cannot be directly applied to Sentinel-2 images. Thus, further development of new algorithms for Sentinel-2 aerosol retrieval over urban areas is critically needed.

In this paper, we developed a new approach to retrieve 60 m spatial resolution AODs from Sentinel-2 images over urban areas. To improve the estimation of surface reflectance, two algorithms for the vegetated areas and the bright areas were employed respectively: (1) the new VIS/2.19 μm surface reflectance relationships as a function of

normalized difference vegetation index (NDVI); and (2) the surface reflectance database preconstructed from the operational high-quality and high-resolution Landsat 8 surface reflectance products. Then Sentinel-2 images covering the period 2018–2019 were collected to perform aerosol retrieval experiments using this new algorithm. The Sentinel-2 retrieved AODs were validated against the Aerosol Robotic Network (AERONET) measurements and compared with MODIS standard aerosol products (MOD04_L2 and MCD19A2) to verify the reliability.

2. Data introduction

2.1. AERONET data sets and study area

The Sun photometers of AERONET provide a comprehensive data set of globally distributed aerosol properties, including the AOD, volume size distribution, single scattering albedo, asymmetry parameter, phase functions, and spectral complex refractive index (Holben et al., 2001; Smirnov et al., 2000). These long-term data (recorded since 1993) cover a wide range of UV/VIS to near-infrared (NIR) channels (0.34–1.02/1.64 μm) with a high temporal resolution of 15 min during midday (Holben et al., 1998; Levy et al., 2007b; Wei et al., 2017). In this work, AERONET version 3 AOD measurements were collected and used to quantitatively evaluate the reliability of the satellite retrieved AODs. Considering AERONET does not provide AOD measurements at 550 nm, the Ångström exponent algorithm was used to interpolate the AOD measurements of the two wavelengths nearest to 550 nm: 440 nm and 675 nm (Ångström, 1964).

With the rapid development of the economy, China has been experiencing severe air pollution problems. Beijing, the capital of China, has consistently been a hotspot for atmospheric pollution research. As shown in Fig. 1, this region consists of complex land use types, such as the grassland, forest, farmland, bare land, and urban. In particular, central Beijing is a typically bright urban area where four AERONET sites are located. In this work, Beijing was selected as the study area, as an example of a large city with distinct spatial air quality patterns and several AERONET sites available. Data types of AERONET AODs used in this area were: Level 2.0 for Beijing sites, and Level 1.5 for Beijing_PKU, Beijing_CAMS and Beijing_RADI sites.

2.2. Operational satellite products

2.2.1. Sentinel-2 data

Sentinel-2 is a mission of European satellites developed to support vegetation, land cover, and environmental monitor. This mission consists of twin polar-orbiting satellites: Sentinel-2A (launched on June 23, 2015) and Sentinel-2B (launched on March 7, 2017), with each satellite carrying a multispectral instrument (MSI) acquiring 13 spectral bands ranging from VIS to SWIR along a 290 km wide orbital swath. The revisit time for each Sentinel-2 satellite is 10 days, which with both satellites combined is reduced to 5 days. The European Space Agency (ESA)

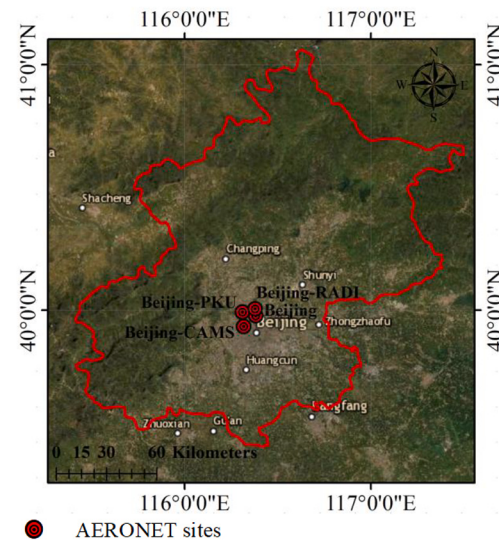


Fig. 1. Locations of four AERONET ground-based sites in Beijing. Area within the irregular red line represents Beijing. (For interpretation of the references to colour in this figure legend, the reader is referred to the web version of this article.)

provides free access to Sentinel-2 Level-1C (L1C) products. These L1C products are composed of 100 km by 100 km tiles with radiometric, geometric corrections and orthorectification being applied, and provide TOA reflectance data for users. Because Sentinel-2 L1C products are resampled with different ground sampling distance (GSD) (10 m, 20 m, and 60 m) according to the native resolution of the different spectral bands (Handbook and Tools, 2015), resampling must be applied first to the L1C products to unify the spatial resolution before aerosol retrieval begins. In this work, a total of 48 Sentinel-2 L1C images from 2018 to 2019, with measurements covering the full image (except images of 10 April 2019, 21 March 2019, and 11 March 2019) and a small cloud amount of less than 10% were collected and downsampled to 60 m. Channels used in the retrieval process were 0.49 μm, 0.665 μm, 0.842 μm and 2.19 μm.

2.2.2. Landsat 8 OLI surface reflectance products

Landsat 8 Operational Land Imager (OLI) surface reflectance products, denoted as Landsat Level-2 (L2) data products, are offered by the United States Geological Survey (USGS) to provide estimations of the Landsat 8 OLI surface spectral reflectance. These L2 surface reflectance data are generated from the specialized software Land Surface Reflectance Code (LaSRC) (Campbell and Aarup, 1989). Compared with precursor Landsat series surface reflectance products over AERONET sites, including the Landsat TM Landsat Ecosystem Disturbance Adaptive Processing System (LEDAPS) products, the Landsat ETM+ LEDAPS products, and the Landsat ETM+ Web-enabled Landsat Data (WELD) products, the performances of the Landsat 8 L2 products are either close to or better (Claverie et al., 2015; Eric et al., 2016; Ju et al., 2012). In addition, compared with the widely used MODIS operational surface reflectance products MOD09A1 (500 m), the spatial resolution of Landsat 8 L2 products (30 m) is approximately 17 times higher. Therefore, high-resolution Landsat 8 OLI surface reflectance products were collected and resampled to 60 m to preconstruct the surface reflectance database for Sentinel-2 images in this work. To reduce the contamination of clouds and shadows, only Landsat 8 OLI surface reflectance products with land cloud cover <10% were collected. Furthermore, only pixels with clear terrain, low-confidence clouds, and low-confidence cirrus were used.

2.2.3. MODIS operational aerosol products

The MOD04_L2 data products, denoted as the MODIS Level 2 (L2) product, provide aerosol optical properties, such as AOD and aerosol size distribution at 10 km pixel resolution over the global oceans and a portion of the continents to users. In the latest Collection 6.1 (C6.1), both the DT and DB aerosol retrieval algorithms are used to create this L2 product. In this work, MOD04_L2 C6.1 product with similar overpass time of Sentinel-2 satellite were collected here for comparison purpose. Further, only DT retrievals, DB retrievals, and DT and DB combined retrievals with best quality assurance (QA) were used here (Wei et al., 2019a).

MCD19A2 product is created by the multi-angle implementation of atmospheric correction (MAIAC) algorithm. This fine spatial resolution (1 km) products is produced daily (Lyapustin et al., 2011). In this work, only best quality (QA.CloudMask = Clear, and QA.AdjacencyMask = Clear) retrievals of MCD19A2 were used (Lyapustin and Wang, 2018). Table 1 lists the data sets used in MODIS aerosol products.

Table 1
Data sets used in MODIS aerosol products.

| Dataset | Scientific Data Set | Contents | QA | Resolution |
|----------|--|-------------------------|----|------------|
| MOD04_L2 | Optical_Depth_Land_And_Ocean | DT AODs | 3 | 10 km |
| | Deep_Blue_Aerosol_Optical_Depth_550_Land_Best_Estimation | DB AODs | ≥2 | 10 km |
| | AOD_550_Dark_Target_Deep_Blue_Combined | DT and DB combined AODs | 3 | 10 km |
| MCD19A2 | Optical_Depth_055 | AODs | | 1 km |

3. Methodology

The radiance received by the satellite at the top of the atmosphere is contributed by the scattering of the atmosphere (i.e. molecules and aerosols), and the reflecting of the underlying surface. As a result, under the assumption that the underlying surface is Lambertian and homogeneous, the reflectance at the top of the atmosphere can be estimated as follows (Eq. (1)):

$$\rho(\lambda, \theta_s, \theta_v, \varphi) = \rho_a(\lambda, \theta_s, \theta_v, \varphi) + \frac{T(\theta_s)T(\theta_v)\rho_s(\lambda, \theta_s, \theta_v, \varphi)}{1 - S_\lambda\rho_s(\lambda, \theta_s, \theta_v, \varphi)} \quad (1)$$

where $\rho(\lambda, \theta_s, \theta_v, \varphi)$ is the TOA reflectance; $\rho_a(\lambda, \theta_s, \theta_v, \varphi)$ represents the atmospheric path reflectance, including aerosol and molecular contributions; $T(\theta_s)$ and $T(\theta_v)$ are the transmission of the atmosphere along the Sun surface path and the surface sensor path, respectively; S_λ is the atmospheric backscattering ratio; $\rho_s(\lambda, \theta_s, \theta_v, \varphi)$ is the surface reflectance; λ represents the wavelength; and θ_s , θ_v , and φ are the solar zenith angle, view zenith angle, and relative azimuth angle, respectively.

Before aerosol retrieval processing begins, radiometric calibration must be applied to Sentinel-2 L1C products to convert the digital number (DN) values into TOA reflectance. An overview of the proposed aerosol retrieval algorithm for Sentinel-2 images is shown in Fig. 2. Because the presence of cloud, cloud shadows, water, and snow impacts the retrieval accuracy severely, process of cloud, cloud shadows, water, and snow mask was imperative before the retrieval processing begins. In this work, the scene classification (SC) maps of Sen2Cor produced Sentinel-2 L2A products were used for this purpose. Then, for a given pixel, its surface reflectance was determined by one of two different methods: (1) the new VIS/2.19 μm surface reflectance relationships as a function of NDVI, and (2) surface reflectance database preconstructed from the high-quality and high-resolution Landsat 8 OLI surface reflectance products, depending on its TOA reflectance at 2.19 μm and the NDVI (channels of 0.665 μm and 0.842 μm). As with most operational aerosol retrieval algorithms, the look-up table (LUT) was employed to store the atmospheric parameters as well as match the appropriate AOD values. Finally, combining the estimated surface reflectance and LUT, AOD can be retrieved from Sentinel-2 images. In this work, channels of 0.49 μm and 0.665 μm, with a spatial resolution of 60 m were used to retrieve AOD at 550 nm.

3.1. Contaminated pixels mask

Pixels such as cloud, cloud shadows, water, and snow can lead to enormous errors in aerosol retrieval. Therefore, such contaminated pixels must be carefully masked before aerosol retrieval. In this work, the SC maps were used for this purpose. The SC map is one of main outputs of the Sen2Cor produced Sentinel-2 Level-2A (L2A) product (Louis et al., 2019), consisting of a total of 12 classifications for shadows, cloud shadows, vegetation, soils/deserts, water, and snow. For each classification, a unique colour and number are assigned to label it. In this work, only classifications in SC maps of dark area, vegetation, and nonvegetation were recognized as the uncontaminated pixels. Examples of the masked Sentinel-2 images using the L2A SC maps are presented in Fig. 3, where Fig. 3 (a) and (c) are Sentinel-2 standard true colour images, and Fig. 3 (b) and (d) are the corresponding masked images. Although there were a few uncontaminated pixels misclassified, contaminated pixels, such as water and thin cloud, were well recognized

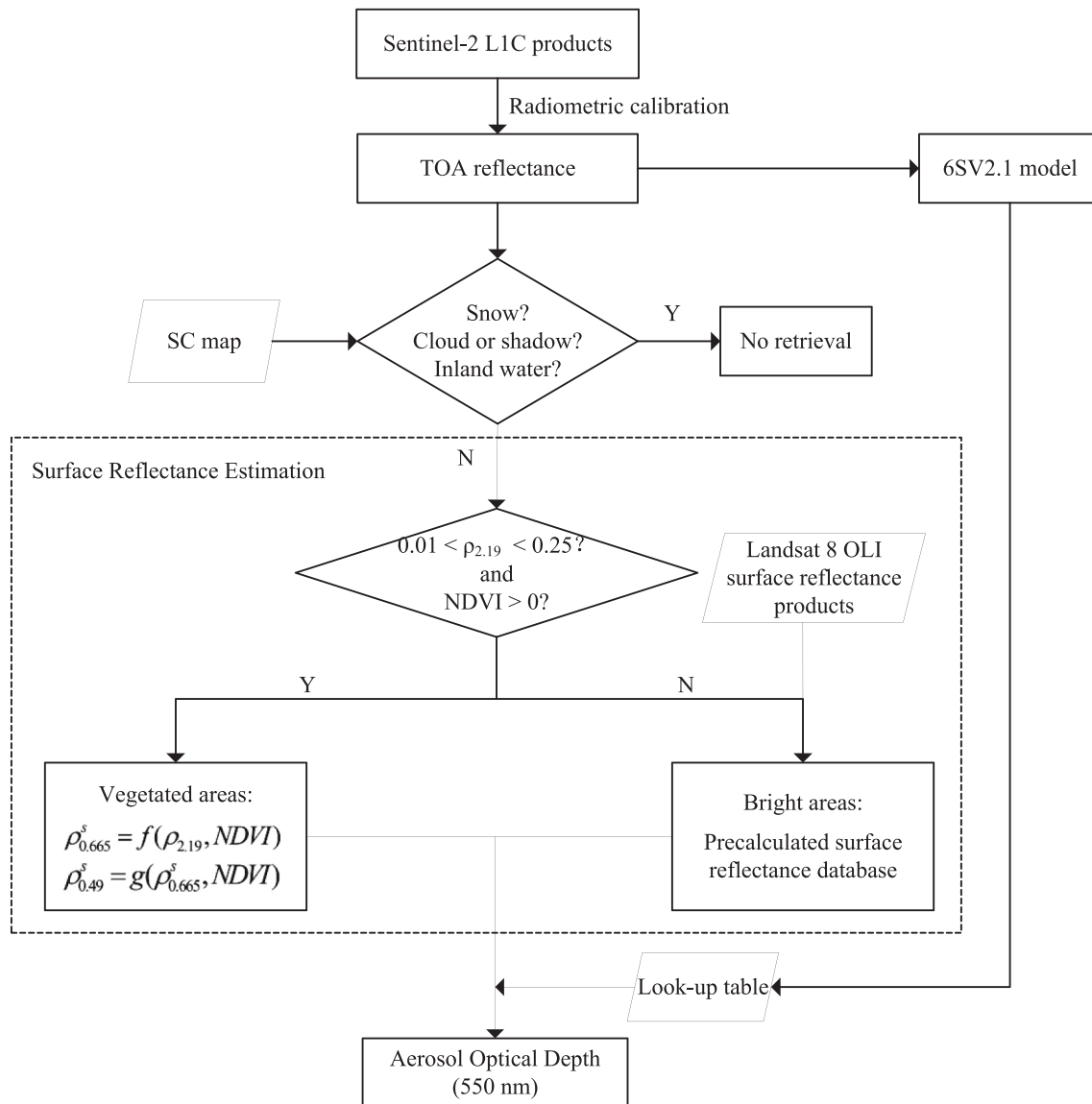


Fig. 2. Flowchart of the high-resolution aerosol retrieval algorithm for Sentinel-2 images.

and masked by the SC maps. Therefore, the Sentinel-2 images with contaminated pixels being masked were then employed to retrieve AOD.

3.2. Surface reflectance estimation

The quality of AOD retrieval from satellite measurements crucially depends on the ability to estimate surface reflectance. Therefore, developing an effective estimation method for the underlying surface reflectance is of great importance. Previous studies have shown that dynamic land surface variations have a negative impact on the estimation of surface reflectance (Hsu et al., 2013; Wei et al., 2018). Thus, to improve the estimation of surface reflectance over complex surfaces, a common method is to estimate the surface reflectance depending on the surface types. In this work, the same strategy was employed here for the estimation purpose. We divided complex urban areas into two categories: (1) the vegetated areas and (2) the bright areas. For each category, a different approach was used to estimate the surface reflectance.

3.2.1. Vegetated areas

The well-known DT algorithm has been confirmed to have good performance in retrieving aerosol properties over densely vegetated

areas, with stable ratios of surface reflectance between VIS and 2.1 μm (Kaufman et al., 1997a). Later, some studies further improved the accuracy of the DT algorithm with modified VIS/2.1 μm empirical surface reflectance ratios (Chander et al., 2009; Gupta et al., 2016; Levy et al., 2007b; Remer et al., 2005). Therefore, the same approach was selected here for aerosol retrieval over vegetated areas. In this work, vegetated areas were defined as TOA reflectance at 2.19 μm ranging between 0.01 and 0.25, as well as NDVI > 0.

Considering the differences in spectral channels and spectral response functions among different sensors, the VIS/2.1 μm surface reflectance relationships for Sentinel-2 measurements were amended. This task was accomplished by collocating Sentinel-2 TOA reflectance measurements in the visible (0.49 μm and 0.665 μm) and SWIR (2.19 μm) channels within a sampling window (3 by 3 pixels) centered on the AERONET site with corresponding ground-based AERONET AOD measurements. The satellite-derived surface reflectance at visible wavelength were then obtained using the collected AERONET AODs to perform atmospheric correction with the Second Simulation of a Satellite Signal in the Solar Spectrum-Vector Version (6SV) model (Vermote et al., 2006). Because the uncertainty of deriving surface reflectance increases significantly as aerosol loading becomes larger, AERONET

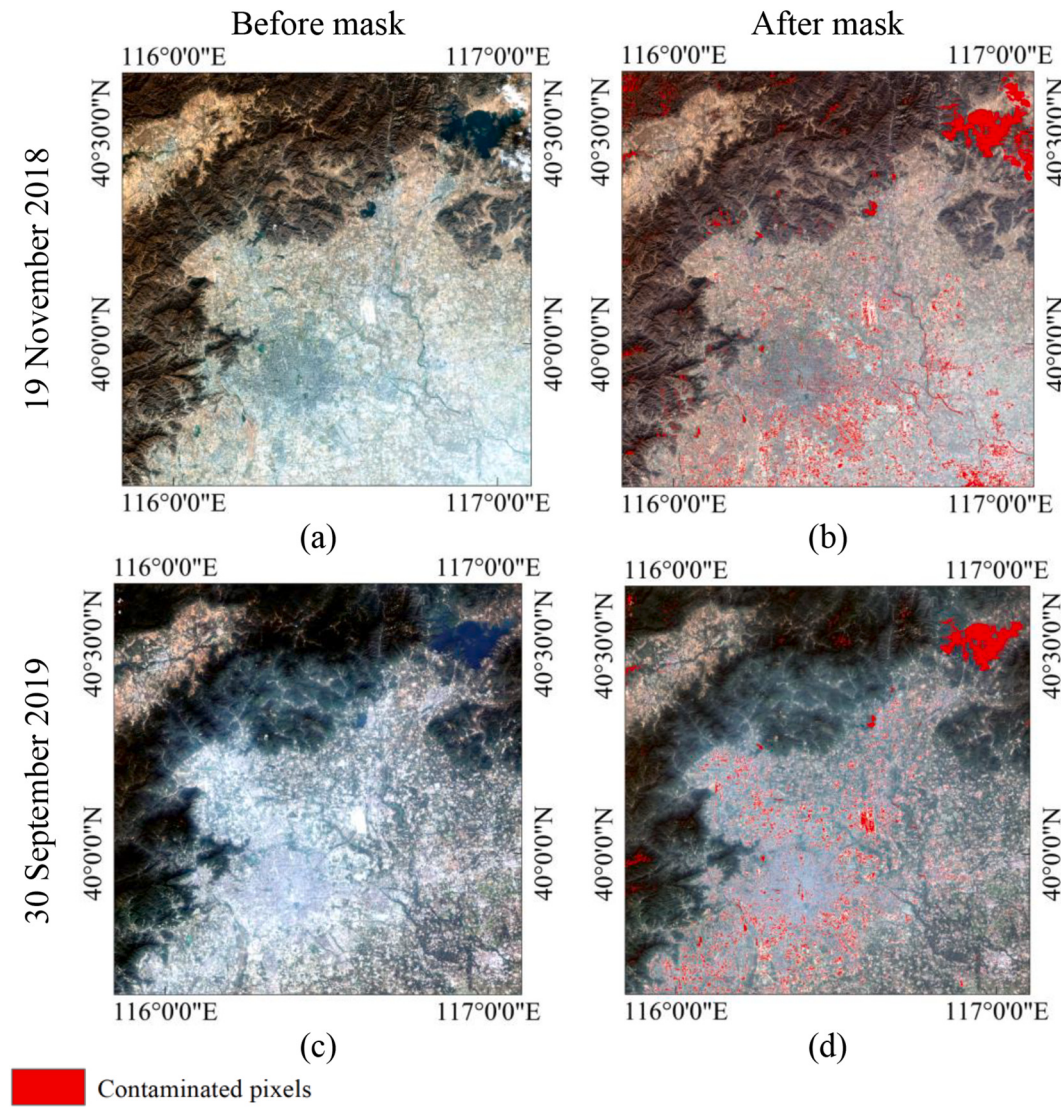


Fig. 3. Sentinel-2 true colour images and corresponding masked images in the Beijing area.

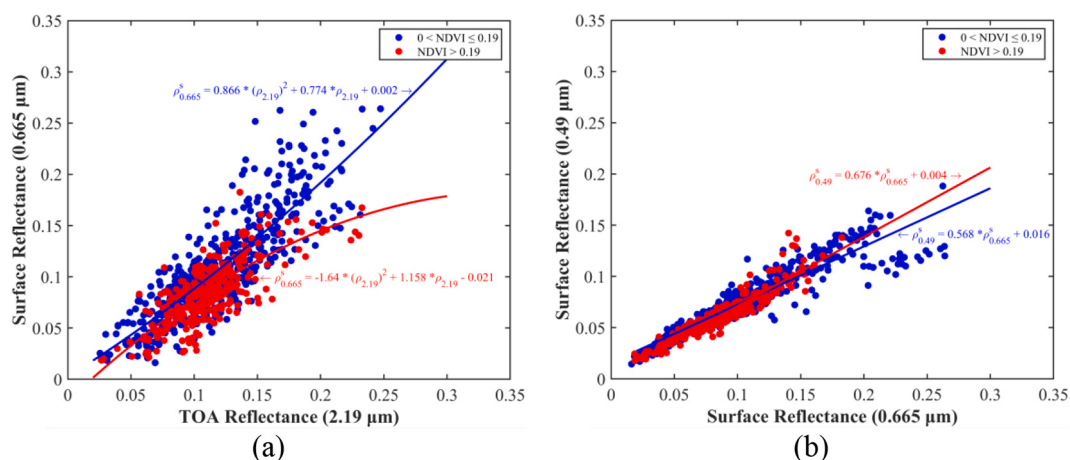


Fig. 4. Sentinel-2 derived spectral surface reflectance relationships (a) between 0.665 μm and 2.19 μm and (b) between 0.49 μm and 0.665 μm as a function of NDVI. The blue and red solid lines represent fitting lines of different NDVI groups. (For interpretation of the references to colour in this figure legend, the reader is referred to the web version of this article.)

data with AOD at $0.55 \mu\text{m} \geq 0.5$ were not processed in this work (Hsu et al., 2013). In order to further eliminate the influence of vegetation variations, the new surface reflectance relationships took vegetation index into account. Pixels over vegetated areas were divided into two different NDVI groups: $0 < \text{NDVI} \leq 0.19$, and $\text{NDVI} > 0.19$. Hereinafter, the new VIS/2.19 μm surface reflectance relationships for each NDVI group were then explored.

The new surface reflectance relationships between visible and SWIR channels can be expressed as the following formulas (Eqs. (2) and (3)):

$$\rho_{0.665}^s = a \times (\rho_{2.19})^2 + b \times \rho_{2.19} + c \quad (2)$$

$$\rho_{0.49}^s = d \times \rho_{0.665}^s + e \quad (3)$$

where $\rho_{2.19}$ is the TOA reflectance at $2.19 \mu\text{m}$; ρ_λ^s is the estimated surface reflectance at wavelength λ ; a , b , c , d , and e are coefficients determined by least squares fitting of the satellite-derived surface reflectance. The spectral surface reflectance relationships given by the above formulas can vary depending upon the NDVI.

Examples of the derived spectral surface reflectance relationships in the study area are provided in Fig. 4. Apparently, caused by vegetation variations, surface types, and seasons, the surface reflectance relationships of these two NDVI groups were quite different. In particular, the red/SWIR surface reflectance relationships were found to be more sensitive to NDVI variation than the blue/red surface reflectance relationships. It could also be seen that as the reflectance increased, the difference in surface reflectance relationships between these two NDVI groups became larger, indicating that this NDVI classification strategy effectively reduced the estimation errors caused by vegetation changes, especially at high $\rho_{2.19}$ ($\rho_{2.19} > 0.15$). To validate the fit, comparisons between the estimated surface reflectance and the satellite-derived atmospheric correction surface reflectance at red/blue channel are presented in Fig. 5. The estimated surface reflectance agreed reasonably with the derived atmospheric correction surface reflectance, with root mean square errors (RMSEs) of 0.023 and 0.017, and correlations of 0.843 and 0.795 for red and blue channels, respectively. As a result, the new surface reflectance relationships for Sentinel-2 measurements were updated and then used to estimate the surface reflectance for visible channels over the defined vegetated areas.

3.2.2. Bright areas

Retrieval of aerosol properties over bright areas is an urgent issue to be solved in this work. However, the unstable VIS/SWIR surface reflectance relationships over bright reflecting areas make the widely

used DT and DT-derived algorithms have many shortcomings (Gupta et al., 2016). Research has shown that the surface reflectance over bright areas is larger than that over vegetated areas (Hsu et al., 2004), and is relatively invariant with time. In addition, the effect of bidirectional reflectance distribution function (BRDF) over bright reflecting areas is also weaker than that over vegetated areas (Hsu et al., 2006). Therefore, it can be safely assumed that the surface reflectance over bright areas with sparse or little vegetation coverage changes little in a short temporal window, and can be estimated from precalculated surface reflectance database.

The minimum reflectivity technique (MRT) is a popular method for preconstructing the surface reflectance database (Herman and Cesarier, 1997; Koelemeijer et al., 2003). With a sequence of satellite images, MRT synthesizes the surface reflectance database from minimum or clearest reflectance pixels. The ESA produced Sentinel-2 Level-2A (L2A) bottom of atmosphere (BOA) reflectance product seems to be an optimal option for preconstructing the surface reflectance database for Sentinel-2 images using the MRT. However, it has been offline at the official website, and users cannot access it directly. Using the freely available Sen2Cor processor (provided by the Sentinel-2 Mission Performance Center at <http://step.esa.int/main/snap-supported-plugins/sen2cor/>), users can produce these L2A products themselves. However, this step is a bit cumbersome and time-consuming. More importantly, research has demonstrated that the performance of the Sen2Cor produced L2A surface reflectance products is poor on aerosol retrieval (Li et al., 2018). Therefore, it is not optimal to use the Sen2Cor produced Sentinel-2 L2A products to preconstruct the surface reflectance database. The widely used MODIS produced surface reflectance product MOD09A1, because of the high temporal resolution (8-days) and reliable quality, is a good candidate for this purpose. However, its coarse spatial resolution (500 m) fails to meet the requirement of high spatial resolution. Therefore, the rigorously validated Landsat 8 L2 surface reflectance products with superior 30 m spatial resolution were selected here instead. Considering the temporal resolution of Landsat 8 L2 products (16 days) somehow may not satisfy the MRT-required quantity in a short temporal window, and the demand of low land cloud cover to decrease the influence of cloud further exacerbate this difficulty, a simpler method of preconstructing the surface reflectance database was proposed. As we all know, the shorter the temporal window is, the less the surface properties change. Thus, we assumed that the surface reflectance of the same target on two images with the closest overpass time (<3 months) is invariable. Based on this assumption, surface reflectance database for a given Sentinel-2 image can be preconstructed from the Landsat 8 OLI surface reflectance product closest to its overpass time.

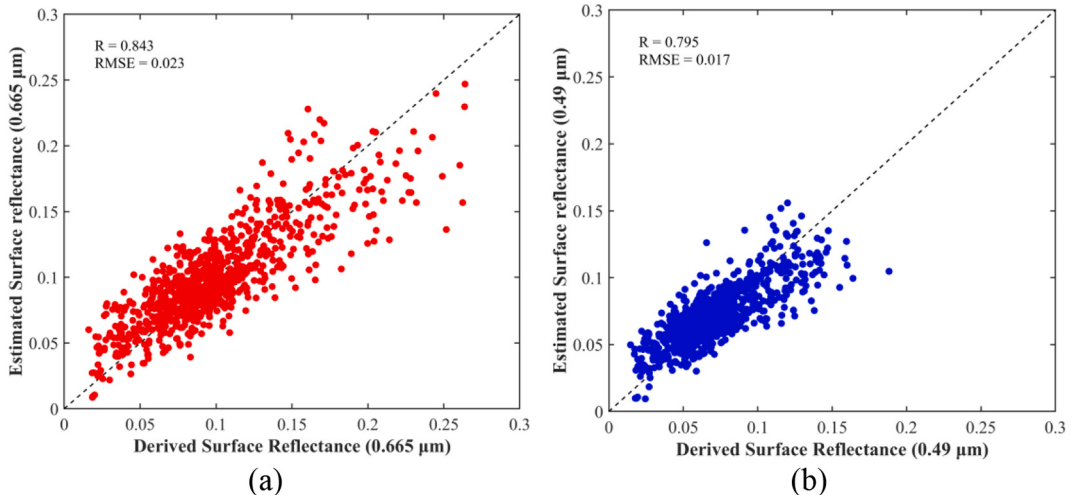


Fig. 5. Comparisons between the derived surface reflectance and estimated surface reflectance for the (a) $0.665 \mu\text{m}$ and (b) $0.49 \mu\text{m}$ channels. The black dashed lines denote the 1:1 lines.

Considering the difference in the detector-averaged relative spectral response function between Sentinel-2 and Landsat 8 OLI may result in differences in the surface reflectance of the same target on the two sensors, Landsat 8 OLI surface reflectance were corrected before using. The correction was accomplished by linear regression of the surface reflectance between Sentinel-2 and Landsat 8 OLI of visible channels as follows:

$$\rho_{\text{Sentinel2}}^s = a \times \rho_{\text{OLI}}^s + b \quad (4)$$

where $\rho_{\text{Sentinel2}}^s$ and ρ_{OLI}^s are surface reflectance of Sentinel-2 and Landsat 8 OLI, respectively; a and b are linear fitting coefficients. Surface reflectance ($\rho_{\text{Sentinel2}}^s$ and ρ_{OLI}^s) were computed by integrating the monochrome reflectance with filter response functions according to:

$$R = \frac{\int_{\lambda_1}^{\lambda_2} S(\lambda) R(\lambda) d\lambda}{\int_{\lambda_1}^{\lambda_2} S(\lambda) d\lambda} = \frac{\sum_{i=0}^{N-1} S(\lambda_i) R(\lambda_i) d\lambda}{\sum_{i=0}^{N-1} S(\lambda_i) d\lambda} \quad (5)$$

where $S(\lambda_i)$ is filter response function at wavelength λ_i ; $R(\lambda_i)$ is spectral reflectance at wavelength λ_i ; λ_1 and λ_2 are the lower and upper limits of wavelengths, respectively. To calculate Eq. (5), standard spectral library, such as the United States Geological Survey (USGS) and John Hopkins University (JHU), from the Environment for Visualizing Images (ENVI) were used. A total of 56 typical objects were used in this work, including vegetation, water, soil and cement.

The calculated linear relationships between Sentinel-2 and Landsat 8 OLI are presented in Fig. 6. In general, the surface reflectance of Sentinel-2 is slightly higher than that of Landsat 8 OLI at visible channels. In addition, the difference in surface reflectance between Sentinel-2 and Landsat 8 OLI is larger in blue channel than in red channel.

Surface reflectance images for the blue channel constructed based on the described algorithms are presented in Fig. 7. It was observed that the overall surface reflectance of the blue channel in the wilting period is significantly higher than that in the lush period, indicating the surface reflectance are susceptible to seasonal change of vegetation growing and dying phases. In addition, surface reflectance was found to be higher over urban areas than over vegetated areas. The estimated surface reflectance images were then used to retrieve AOD over the study area.

3.3. Look-up table

As with most operational aerosol retrieval algorithms, a

precalculated LUT is necessary (Levy et al., 2007a). In this work, the widely used and rigorously validated 6SV model was selected to pre-construct the LUT. Compared with the previous 6S model, the 6SV model accounts for the effect of polarization for including the calculation of four components of the Stokes vector, characterizing the intensity of radiation, and perpendicular, parallel, and elliptical polarization. In addition, compared with other radiative transfer (RT) codes, the 6SV model has been found to provide users with a relative average accuracy of approximately 0.4–0.6% (Vermote et al., 2006).

A deep understanding of the aerosol model is another particularly difficult and critical component in developing a satellite aerosol retrieval algorithm (Levy et al., 2007b). The 6SV model provides five default aerosol models for users, including continental model, maritime model, urban model, desert model, and biomass burning smoke model. With these five default models, aerosol conditions in most regions of the world can be described. Previous research show that the continental aerosol model can broadly describe the aerosol condition for Beijing (He et al., 2015; Sun et al., 2010; Sun et al., 2016; Wang et al., 2012). Therefore, the continental aerosol model was selected here for AOD retrieval. The optical properties of the continental model, as reported in Vermote et al., are listed in Table 2 (Vermote et al., 2006). Finally, with parameters such as AOD values (0.0 to 2.0, with an increment of 0.01), geometrical conditions (=MTD_TL.xml files in the Sentinel-2 L1C products), atmospheric conditions (mid-latitude summer model and mid-latitude winter model), aerosol model (continental model), land surface reflectance (=0) and spectral response functions for Sentinel-2 input into the 6SV model, the LUT under different observations was constructed before aerosol retrieval. For more details about the 6SV model please refer to <http://6s.ltdri.org>.

4. Results and discussion

4.1. Evaluation source and approaches

To increase the number of statistical samples and account for the spatial variability imposed by atmospheric motion, the average value of the satellite retrieved AODs within a sampling window (5 × 5 pixels) centered on the AERONET site was used as the satellite retrieval at this site (Bilal et al., 2017; Ichoku et al., 2002; Wei, 2018). Average of AERONET measurements within ±30 min of the satellite overpass times was used as the ground truth (Hsu et al., 2006; Hsu et al., 2004; Kaufman et al., 1997a; Levy et al., 2007a; Levy et al., 2007b). Retrieval errors are reported as the RMSE, the mean absolute error (MAE), and the expected

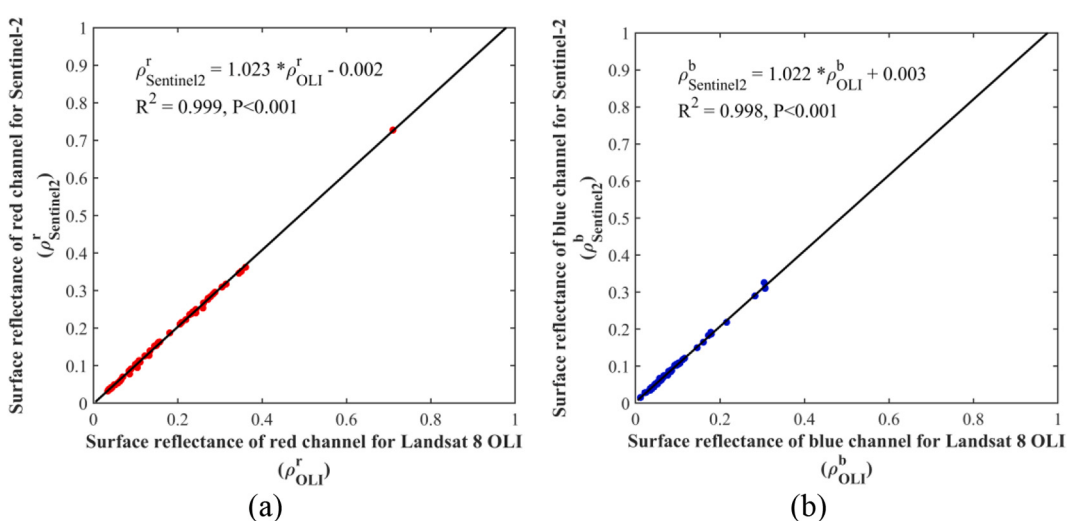


Fig. 6. The linear regression analysis of Sentinel-2 and Landsat 8 OLI surface reflectance in (a) red and (b) blue channel. Black solid lines represent regression lines. (For interpretation of the references to colour in this figure legend, the reader is referred to the web version of this article.)

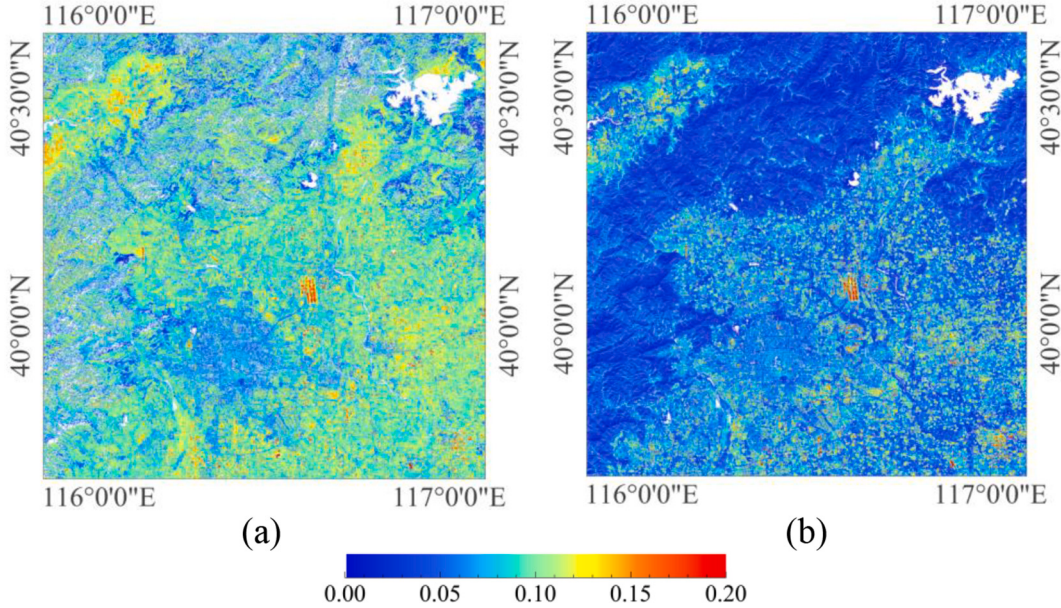


Fig. 7. Sentinel-2 surface reflectance images at blue channel ($0.49\text{ }\mu\text{m}$) in the Beijing area. (a) 19 November 2018, and (b) 30 September 2019. Gaps represent masked contaminated pixels. (For interpretation of the references to colour in this figure legend, the reader is referred to the web version of this article.)

Table 2

Optical properties of the continental model used in AOD retrieval at 550 nm.

| Model | Component | r_v | σ | C_j | RP-CRI | IP-CRI | ω | g |
|-------------|---------------|-------|----------|-------|--------|--------|----------|-------|
| Continental | Dust-like | 17.6 | 1.09 | 0.70 | 1.530 | 0.008 | 0.893 | 0.634 |
| | Water-soluble | 0.170 | 1.09 | 0.29 | 1.530 | 0.006 | | |
| | Soot | 0.050 | 0.69 | 0.01 | 1.750 | 0.440 | | |

Note: r_v , σ , and C_j represent the mean radius (μm), standard deviation for the size distribution parameters, and volume percentages; RP-CRI, IP-CRI, ω , and g stand for the real and imaginary parts of the refractive index, the single scattering albedo, and asymmetry factor, respectively.

error (EE) to measure the differences between satellite retrieved AODs and AERONET measured AODs. These error measurements are defined as follows (Eqs. (6), (7), and (8)):

$$\text{RMSE} = \sqrt{\frac{1}{n} \sum_{i=1}^n \left((\text{AOD})_i^{\text{satellite}} - (\text{AOD})_i^{\text{AERONET}} \right)^2} \quad (6)$$

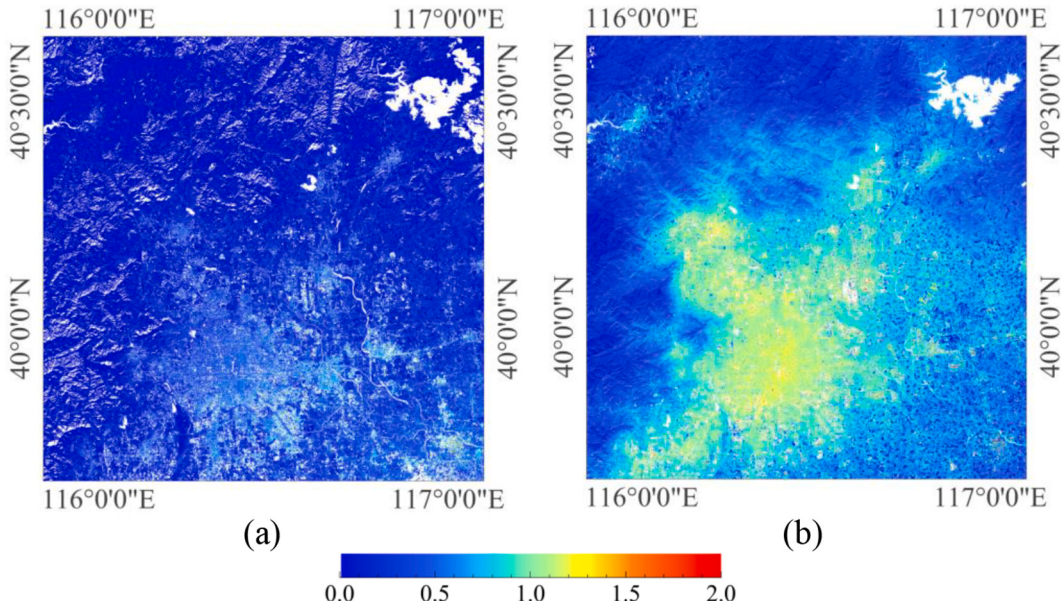


Fig. 8. Retrieved AOD at 550 nm for partial Sentinel-2 images; (a) 19 November 2018 and (b) 30 September 2019. Gaps represent contaminated pixels.

$$\text{MAE} = \frac{1}{n} \sum_{i=1}^n |(\text{AOD})_i^{\text{satellite}} - (\text{AOD})_i^{\text{AERONET}}| \quad (7)$$

$$\text{EE} = \pm (0.05 + 0.2 \times (\text{AOD})^{\text{AERONET}}) \quad (8)$$

$$(\text{AOD})^{\text{AERONET}} - |\text{EE}| \leq (\text{AOD})^{\text{satellite}} \leq (\text{AOD})^{\text{AERONET}} + |\text{EE}| \quad (9)$$

where $(\text{AOD})^{\text{satellite}}$ is the satellite retrievals, and $(\text{AOD})^{\text{AERONET}}$ is the AERONET retrievals. When satellite retrieved AODs fall within the defined envelope (Eq. (9)), they can be considered as good matches. The

correlation coefficient (R) was also selected here to indicate the agreement between the satellite retrieved AODs and AERONET measured AODs, with linear regression to estimate the slope and intercept.

4.2. Results

We used the algorithm described above to retrieve high resolution AODs from Sentinel-2 measurements. There were total of 48 Sentinel-2 L1C images from 2018 to 2019, with land cloud cover less than 10% collected. Fig. 8 shows examples of our retrievals at 60 m spatial

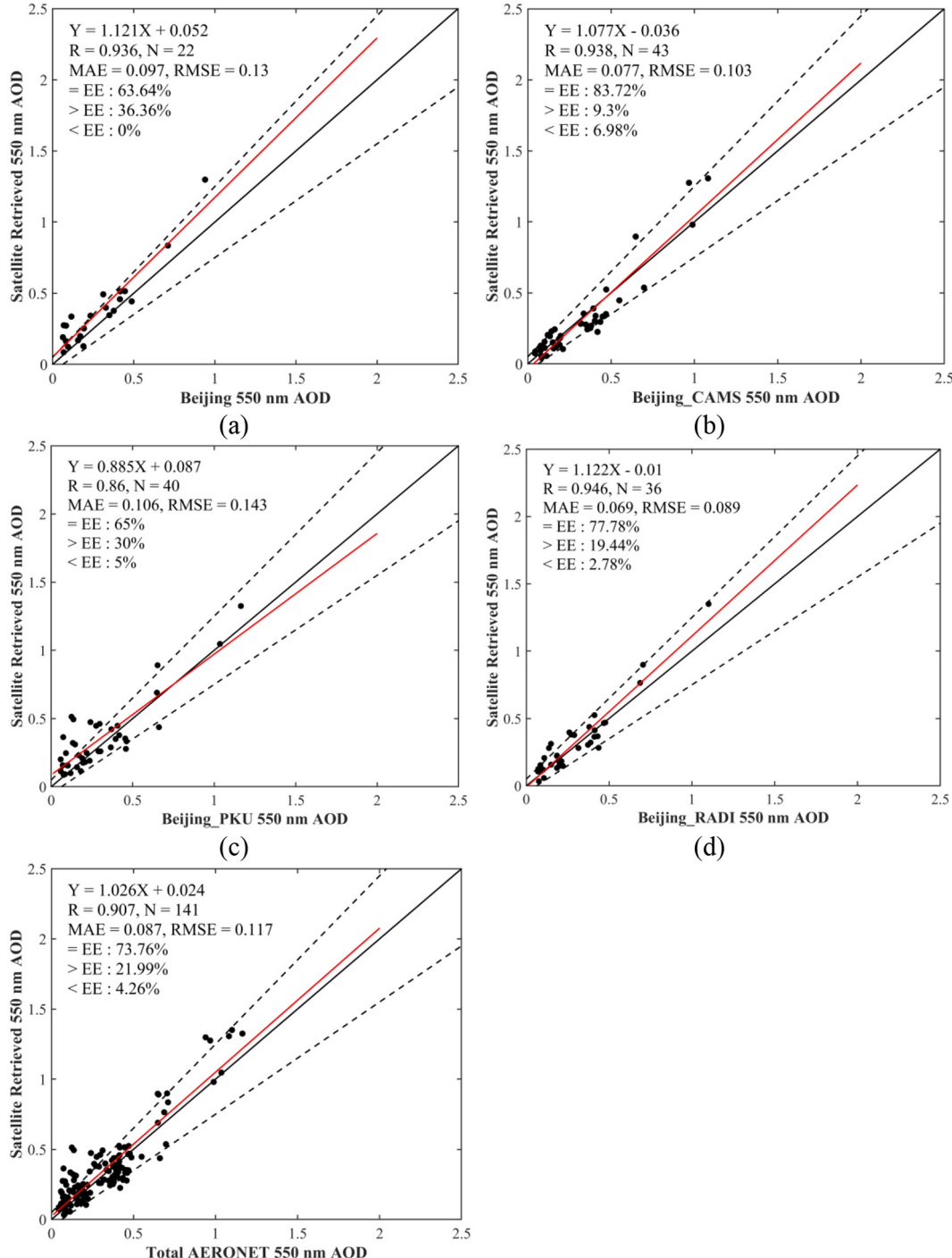


Fig. 9. Validation of the Sentinel-2 AOD retrievals against AERONET AOD measurements at 550 nm. (a) Beijing site, (b) Beijing_CAMS site, (c) Beijing_PKU site, (d) Beijing_RADI site, and (e) total AERONET site in the study area. The dotted lines represent EE lines, the black solid lines represent 1:1 lines, and the red solid lines represent regression lines. (For interpretation of the references to colour in this figure legend, the reader is referred to the web version of this article.)

resolution over the study area on (a) 19 November 2018 and (b) 30 September 2019, where gaps represent masked contaminated pixels. It was observed that the proposed algorithm was able to provide continuous and detailed 60 m AOD distributions over both vegetated and bright areas. In addition, the surrounding areas were found to show overall lower AOD values than those of the centers of urban areas, which was consistent with the reality. It was also found that most of the aerosol loadings in the study area were lower than 1.5. Retrievals in the lush period (Fig. 8 (b)) were found to be significantly higher than that in the wilting period (Fig. 8 (a)), indicating that the study area suffered serious pollution around 30 September 2019. Because of the sustained variations of surface information, the complex urban surface, and the usage of two different methods for estimation the surface reflectance, noise and fluctuation were unavoidable in the retrievals, resulting in the dark blue “dots” in Fig. 8 (b).

4.3. Validation with AERONET AOD measurements

AOD measurements from AERONET stations were used to validate the high-resolution satellite retrieved AODs from Sentinel-2 images. Fig. 9 shows the validation of the retrieved AODs from the proposed algorithm against AERONET AODs in the study area. The black solid lines represent the 1:1 lines, the black dotted lines are the EE lines, and the red solid lines are the regression lines.

It is apparent that the Sentinel-2 AOD retrievals agreed well with the AERONET AODs at the Beijing_CAMS site (Fig. 9 (b)), with a high correlation coefficient ($R = 0.938$) and highest EE (83.72%), and small values of MAE (0.077) and RMSE (0.103). Similar good agreement of the Sentinel-2 AOD retrievals was also found in the Beijing_RADI site, as shown in Fig. 9 (d). AOD retrievals for this site showed correlation with AERONET measurements as high as 0.946, and near 80% falling within EE, whereas the MAE and RMSE values were as low as 0.069 and 0.089, respectively. Caused by the overestimation, EEs for the Beijing and Beijing_PKU sites were found to be relatively low. However, with correlation coefficients larger than 0.85, and more than 60% of AODs fell within EE, it demonstrated that the Sentinel-2 retrieved AODs reasonably consistent with the AERONET AODs at these two sites. Fig. 9 (e) provides a scatterplot of all the Sentinel-2 retrieved AODs and AERONET AODs from all four sites across the study area. Overall, with a total of 73.76% AOD retrievals falling within the confidence envelope, a correlation coefficient of 0.907, and overall MAE and RMSE of 0.087 and 0.117, respectively, it implies that the proposed algorithm performed well in high spatial resolution AOD retrieval over Beijing, and can accurately retrieve AODs from Sentinel-2 images.

Comparisons of the Sentinel-2 retrieved AODs in different seasons are shown in Table 3. It was found that AODs from the proposed algorithm agreed best with AERONET measurements in Winter, with correlation coefficient higher than 0.95, EE of 90%, and MAE and RMSE values as low as 0.052 and 0.062, respectively. Similar good agreement also was found in Autumn, with correlation coefficient as high as 0.97, EE of 74.29%, and MAE and RMSE values of 0.093 and 0.133, respectively. Correlation coefficient in Spring was relatively low ($R = 0.672$); however, near 80% of the AODs fell within EE, indicating that the Sentinel-2 retrieved AODs agreed reasonably with the AERONET measurements. Retrievals of the proposed algorithm in Summer were poor, with less than 50% within EE. Reasons can be mainly summarized into

two aspects: (1) the quantity of the retrievals in Summer were relatively small, (2) the estimated surface reflectance is relatively less accurate in Summer caused by the rapid variations of surface types and aerosol model.

4.4. Comparison with MODIS aerosol products

Examples of the comparisons of the proposed algorithm retrieved AODs and MOD04_L2 AOD products against AERONET AOD measurements is shown in Fig. 10. Compared with the DT retrieved AODs, AODs from the proposed algorithm were slightly superior, with higher EE, and approximate MAE. Overestimation were found in both two retrievals; however, compared with the MOD04_L2 DT retrievals, the Sentinel-2 retrievals were more acceptable with much lower > EE percentage.

It was found that MOD04_L2 DB retrievals showed good agreement with AERONET measurements, with correlation coefficient of 0.823, and EE of 74.42%; however, MAE and RMSE were relatively high (0.097 and 0.154, respectively). As shown in Fig. 10 (d), two heavily overestimated retrievals were found in the DB retrievals, significantly contributing to the high MAE and RMSE values. Compared with the MOD04_L2 DB retrievals, retrievals from the proposed algorithm achieved a stronger correlation with AERONET measurements ($R = 0.874$), with slightly higher EE, and lower values of MAE and RMSE.

Comparison result of the Sentinel-2 AODs and MOD04_L2 DT and DB combined AODs are shown in Fig. 10 (e) and (f). Due to the combination of the DT and DB retrievals, both overestimation in the DT retrievals and underestimation in the DB retrievals were effectively weakened in the combined retrievals. However, regression slope of the MOD04_L2 combined AODs up to 1.244, deviated from the ratio 1 severely, indicating that as the AOD value increases, retrieval error will become larger rapidly. Apparently, compared with the MOD04_L2 combined AODs, the Sentinel-2 AODs were superior, with higher EE, lower values of MAE and RMSE. Though correlation coefficient of the Sentinel-2 AODs was slightly lower than that of MOD04_L2 combined AODs, regression line of the Sentinel-2 AODs was more reasonable. Overall, the comparison results showed that the proposed algorithm performed better than the routine MOD04_L2 AOD products over Beijing.

An example of the comparison of the proposed algorithm retrieved AODs and fine spatial resolution MCD19A2 AOD products against AERONET AOD measurements is shown in Fig. 11. It was found that the MCD19A2 AOD retrievals showed good agreement with AERONET measurements, with high correlation coefficient ($R = 0.939$), and more than 85% within EE, and low values of MAE and RMSE (0.094 and 0.111, respectively). Compared with the MCD19A2 AODs, the Sentinel-2 AODs was inferior in within EE percentage. However, with near 80% of the retrievals falling within EE, higher correlation coefficient ($R = 0.96$), and lower values of MAE and RMSE (0.085 and 0.108, respectively), it can be concluded that AODs from the proposed algorithm were comparable to the MCD19A2 AODs.

5. Conclusions

In this work, a new algorithm for retrieving AOD from high-resolution Sentinel-2 measurements over urban areas was developed. To improve the estimation of surface reflectance, one of two different methods: (1) the new VIS/2.19 μm surface reflectance relationships as a function of NDVI, and (2) surface reflectance database preconstructed from the high-quality and high-resolution Landsat 8 OLI surface reflectance products, were adopted depending on the surface types. Validation with the AERONET AOD measurements and comparison with the MODIS standard aerosol products (MOD04_L2 and MCD19A2) in Beijing indicated that:

- (1) The proposed algorithm is able to provide continuous and detailed aerosol distributions at 60 m spatial resolution over both bright and vegetated urban surfaces.

Table 3
Comparisons of the Sentinel-2 AODs in different seasons.

| Season | Number | R | EE (%) | >EE (%) | <EE (%) | MAE | RMSE |
|--------|--------|-------|--------|---------|---------|-------|-------|
| Summer | 19 | 0.744 | 36.84 | 57.89 | 5.26 | 0.153 | 0.177 |
| Spring | 57 | 0.672 | 77.19 | 15.79 | 7.02 | 0.079 | 0.103 |
| Autumn | 35 | 0.97 | 74.29 | 25.71 | 0.00 | 0.093 | 0.133 |
| Winter | 30 | 0.955 | 90.00 | 6.67 | 3.33 | 0.052 | 0.062 |

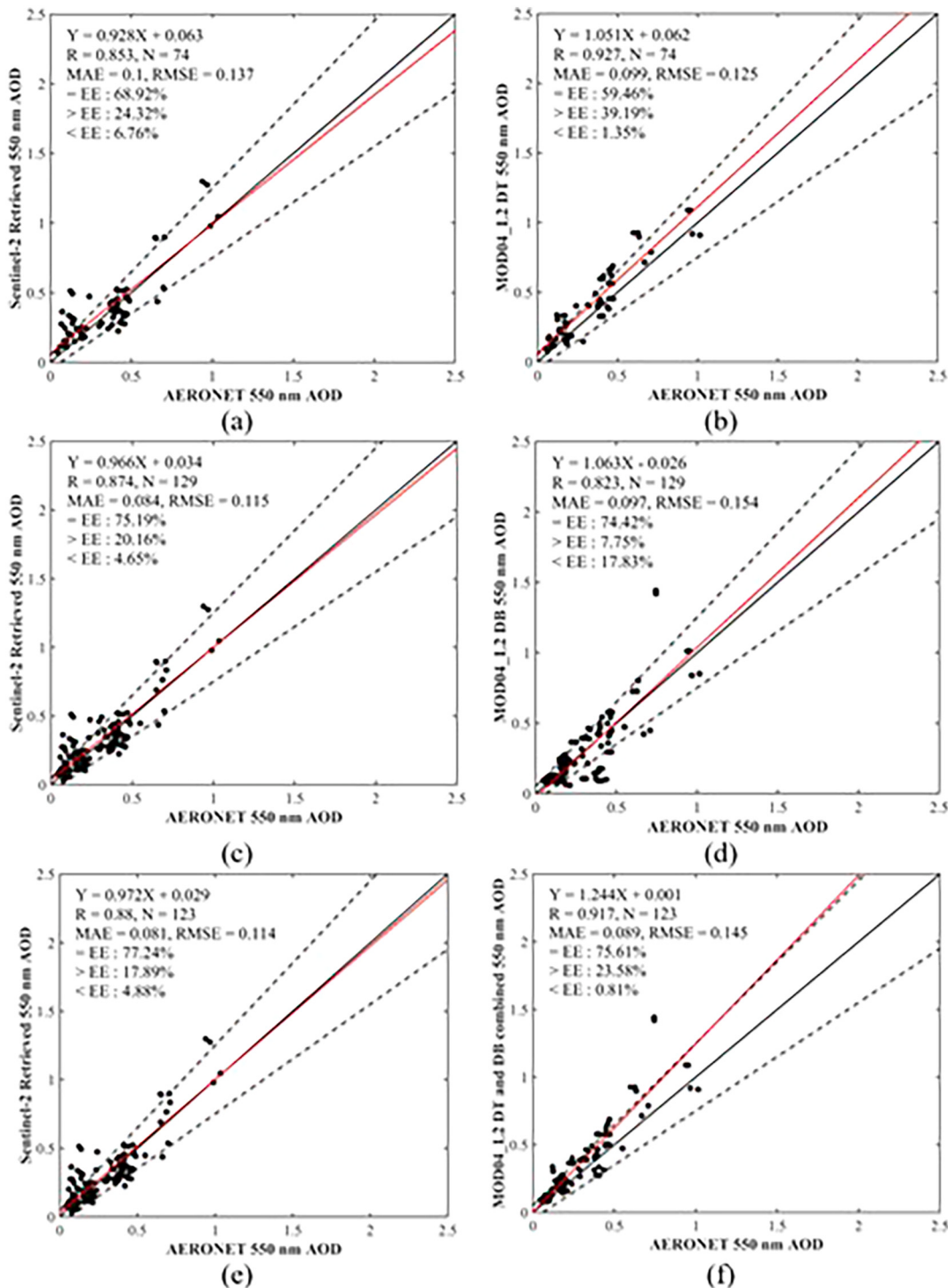


Fig. 10. Comparisons of the Sentinel-2 AOD retrievals with MOD04_L2 aerosol products against AERONET AODs in the study area. (a), (c), and (e) the proposed algorithm retrievals, (b) MOD04_L2 DT retrievals, (d) MOD04_L2 DB retrievals, and (f) MOD04_L2 DT and DB combined retrievals. The dotted lines represent EE lines, the black solid lines represent 1:1 lines, and the red solid lines represent regression lines. (For interpretation of the references to colour in this figure legend, the reader is referred to the web version of this article.)

- (2) Sentinel-2 AOD retrievals have good agreement with AERONET AOD measurements, with correlation coefficient of 0.907, 73.76% of them overall falling within the EE, and low values of MAE (0.087) and RMSE (0.117), indicating that the new algorithm can accurately retrieve AOD at a high spatial resolution from Sentinel-2 measurements.
- (3) The retrievals from the proposed algorithm because of the ability of the Sentinel-2 satellite to provide observations at high revisit

- time (5 days), have the potential to monitor high-resolution aerosol distributions at relatively fine temporal resolution.
- (4) Comparison with routine MOD04_L2 aerosol products (10 km) show that the Sentinel-2 AOD retrievals were superior, and the proposed algorithm performed better over complex urban areas of Beijing.

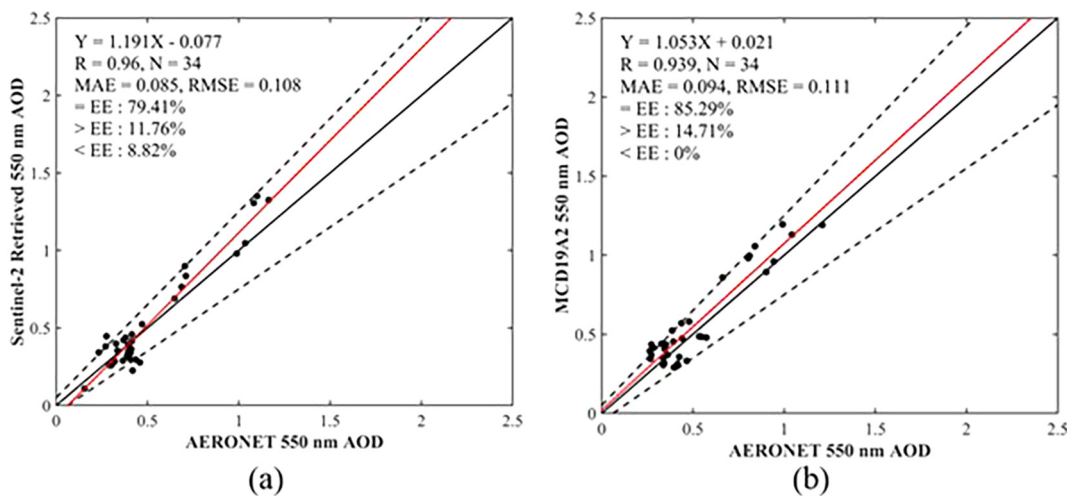


Fig. 11. Comparisons of the Sentinel-2 AOD retrievals with MCD19A2 aerosol products against AERONET AODs in the study area. (a) the proposed algorithm retrievals; (b) MCD19A2 retrievals. The dotted lines represent EE lines, the black solid lines represent 1:1 lines, and the red solid lines represent regression lines. (For interpretation of the references to colour in this figure legend, the reader is referred to the web version of this article.)

(5) Comparison result of the proposed algorithm retrieved AODs and the fine spatial resolution MCD19A2 (1 km) AODs indicates that retrievals of the proposed algorithm were comparable.

As the proposed algorithm partially relies on the preconstructed surface reflectance database, the influences of the temporal changes of surface reflectance should be further explored. In addition, different view/solar geometry and instrument calibration method between the Landsat 8 and Sentinel-2 may also lead errors in the estimation of surface reflectance. We will focus on investigation and discussion these difficulties in future work.

CRediT authorship contribution statement

Yue Yang: Conceptualization, Methodology, Software, Data curation, Writing – original draft, Formal analysis, Validation. **Yunping Chen:** Supervision, Project administration, Writing – review & editing, Funding acquisition. **Kangzhuo Yang:** Visualization, Investigation, Validation. **Jan Cermak:** Writing – review & editing. **Yan Chen:** Resources.

Declaration of Competing Interest

The authors declare that they have no known competing financial interests or personal relationships that could have appeared to influence the work reported in this paper.

Acknowledgements

This work was supported by Sichuan Science and Technology Plan Project (No. 2019YJ0201), the advance research project of civil space technology, National Civil Space Infrastructure Land Observation Satellite Common Application Support Platform (No. Y930280A2F), and the China Scholarship Council (No. 202006070089).

References

- Ångström, A., 1964. The parameters of atmospheric turbidity. *Tellus* 16, 64–75.
- Bilal, M., Nichol, J.E., Bleiweiss, M.P., Dubois, D., 2013. A Simplified high resolution MODIS Aerosol Retrieval Algorithm (SARA) for use over mixed surfaces. *Remote Sens. Environ.* 136, 135–145. <https://doi.org/10.1016/j.rse.2013.04.014>.
- Bilal, M., Nichol, J.E., Wang, L.C., 2017. New customized methods for improvement of the MODIS C6 Dark Target and Deep Blue merged aerosol product. *Remote Sens. Environ.* 197, 115–124. <https://doi.org/10.1016/j.rse.2017.05.028>.
- Campbell, J.W., Aarup, T.J.L., 1989. Oceanography, Photosynthetically available radiation at high latitudes, 34.
- Chander, G., Markham, B.L., Helder, D.L., 2009. Summary of Current Radiometric Calibration Coefficients for Landsat MSS, TM, ETM+, and EO-1 ALI Sensors, 113. *Remote Sens. Environ.*, pp. 893–903
- Clarke, A.D., et al., 2001. Dust and pollution transport on global scales: aerosol measurements and model predictions. *J. Geophys. Res.-Atmos.* 106, 32555–32569. <https://doi.org/10.1029/2000jd900842>.
- Claverie, M., Vermote, E.F., Franch, B., Masek, J.G., 2015. Evaluation of the Landsat-5 TM and Landsat-7 ETM+ Surface Reflectance Products. *Remote Sens. Environ.*
- Deuze, J.L., et al., 2001. Remote sensing of aerosols over land surfaces from POLDER-ADEOS-1 polarized measurements. *J. Geophys. Res.-Atmos.* 106, 4913–4926. <https://doi.org/10.1029/2000jd900364>.
- Diner, D.J., et al., 2005. Using angular and spectral shape similarity constraints to improve MISR aerosol and surface retrievals over land. *Remote Sens. Environ.* 94, 155–171. <https://doi.org/10.1016/j.rse.2004.09.009>.
- Eric, et al., 2016. Preliminary analysis of the performance of the Landsat 8/OLI land surface reflectance product.
- Gupta, P., Levy, R.C., Mattoo, S., Remer, L.A., Munchak, L.A., 2016. A surface reflectance scheme for retrieving aerosol optical depth over urban surfaces in MODIS Dark Target retrieval algorithm. *Atmos. Meas. Tech.* 9, 3293–3308. <https://doi.org/10.5194/amt-9-3293-2016>.
- Handbook, S.U., Tools, E., 2015. Sentinel-2 User Handbook. ESA Standard Document Date 1, 1–64.
- He, J., et al., 2015. Retrieval of aerosol optical thickness from HJ-1 CCD data based on MODIS-derived surface reflectance, 36, pp. 882–898.
- Herman, J.R., Celarier, E.A., 1997. Earth surface reflectivity climatology at 340–380 nm from TOMS data, 102. *J. Geophys. Res.-Atmos.*, pp. 28003–28011
- Holben, B.N., et al., 1998. AERONET - A federated instrument network and data archive for aerosol characterization. *Remote Sens. Environ.* 66, 1–16. [https://doi.org/10.1016/S0034-4257\(98\)00031-5](https://doi.org/10.1016/S0034-4257(98)00031-5).
- Holben, B.N., et al., 2001. An emerging ground-based aerosol climatology: aerosol optical depth from AERONET. *J. Geophys. Res.-Atmos.* 106, 12067–12097. <https://doi.org/10.1029/2001jd000014>.
- Hsu, N.C., Tsay, S.C., King, M.D., Herman, J.R., 2004. Aerosol properties over bright-reflecting source regions, 42. *Ieee T Geosci. Rem.*, pp. 557–569
- Hsu, N.C., Tsay, S.C., King, M.D., Herman, J.R., 2006. Deep blue retrievals of Asian aerosol properties during ACE-Asia. *Ieee T Geosci. Rem.* 44, 3180–3195. <https://doi.org/10.1109/Tgrs.2006.879540>.
- Hsu, N.C., et al., 2013. Enhanced Deep Blue aerosol retrieval algorithm: the second generation, 118.
- Huang, R.J., et al., 2014. High secondary aerosol contribution to particulate pollution during haze events in China. *Nature* 514, 218–222. <https://doi.org/10.1038/nature13774>.
- Ichoku, C., et al., 2002. Analysis of the performance characteristics of the five-channel Microtops II Sun photometer for measuring aerosol optical thickness and precipitable water vapor. *J. Geophys. Res.-Atmos.* 107 <https://doi.org/10.1029/2001jd001302> doi:ArtN 4179.
- Ju, J., Roy, D.P., Vermote, E., Masek, J., Kovalskyy, V., 2012. Continental-scale validation of MODIS-based and LEDAPS Landsat ETM+ atmospheric correction methods, 122. *Remote Sens. Environ.*, pp. 175–184
- Kaufman, Y.J., Wald, A.E., Remer, L.A., Gao, B.C., 1997b. The MODIS 2.1- μm channel-correlation with visible reflectance for use in remote sensing of aerosol. *Trans. Geosci. Rem. Sens. IEEE* 35, 1286–1298.

- Kaufman, Y.J., et al., 1997a. Passive remote sensing of tropospheric aerosol and atmospheric correction for the aerosol effect. *J. Geophys. Res.-Atmos.* 102, 16815–16830. <https://doi.org/10.1029/97jd01496>.
- Kaufman, Y.J., Tanre, D., Boucher, O., 2002. A satellite view of aerosols in the climate system. *Nature* 419, 215–223. <https://doi.org/10.1038/nature01091>.
- Koelemeijer, R.B.A., De Haan, J.F., Stammes, P., 2003. A database of spectral surface reflectivity in the range 335–772 nm derived from 5.5 years of GOME observations, 108. *J. Geophys. Res.-Atmos.*
- Levy, R.C., Remer, L.A., Dubovik, O., 2007a. Global aerosol optical properties and application to Moderate Resolution Imaging Spectroradiometer aerosol retrieval over land. *J. Geophys. Res.-Atmos.* 112 <https://doi.org/10.1029/2006jd007815> doi:Artn D13210.
- Levy, R.C., Remer, L.A., Mattoo, S., Vermote, E.F., Kaufman, Y.J., 2007b. Second-generation operational algorithm: Retrieval of aerosol properties over land from inversion of Moderate Resolution Imaging Spectroradiometer spectral reflectance. *J. Geophys. Res.-Atmos.* 112 <https://doi.org/10.1029/2006jd007811> doi:Artn D13211.
- Li, Z.Q., et al., 2011. Long-term impacts of aerosols on the vertical development of clouds and precipitation. *Nat. Geosci.* 4, 888–894. <https://doi.org/10.1038/NGeo1313>.
- Li, Y., et al., 2018. Evaluation of Sentinel-2A surface reflectance derived using Sen2Cor in North America, 11, pp. 1997–2021.
- Liang, S.L., Zhong, B., Fang, H.L., 2006. Improved estimation of aerosol optical depth from MODIS imagery over land surfaces. *Remote Sens. Environ.* 104, 416–425. <https://doi.org/10.1016/j.rse.2006.05.016>.
- Louis, J., et al., 2019. Sentinel-2 global surface reflectance level-2a product generated with Sen2cor. *Int. Geosci. Rem. Se* 8522–8525.
- Luo, N., Wong, M.S., Zhao, W.J., Yan, X., Xiao, F., 2015. Improved aerosol retrieval algorithm using Landsat images and its application for PM10 monitoring over urban areas. *Atmos. Res.* 153, 264–275. <https://doi.org/10.1016/j.atmosres.2014.08.012>.
- Lyapustin, A., Wang, Y.J.N.G., 2018. MD, USA, MODIS Multi-Angle Implementation of Atmospheric Correction (MAIAC) Data User's Guide.
- Lyapustin, A., et al., 2011. Multiangle implementation of atmospheric correction (MAIAC): 2. Aerosol algorithm, 116.
- Munchak, L., et al., 2013. MODIS 3 Km Aerosol Product: Applications over Land in an Urban/Suburban Region, 6, pp. 1747–1759.
- North, P.R., 2002. Estimation of aerosol opacity and land surface bidirectional reflectance from ATSR-2 dual-angle imagery: operational method and validation, 107. *J. Geophys. Res.-Atmos.*, p. 4149
- Ramanathan, V., et al., 2001. Indian Ocean Experiment: an integrated analysis of the climate forcing and effects of the great Indo-Asian haze. *J. Geophys. Res.-Atmos.* 106, 28371–28398. <https://doi.org/10.1029/2001jd900133>.
- Remer, L.A., et al., 2005. The MODIS aerosol algorithm, products, and validation. *J. Atmos. Sci.* 62, 947–973. <https://doi.org/10.1175/Jas3385.1>. Sentinel, E.J.E.S.D., User Handbook, 64.
- Smirnov, A., Holben, B.N., Eck, T.F., Dubovik, O., Slutsker, I., 2000. Cloud-screening and quality control algorithms for the AERONET database. *Remote Sens. Environ.* 73, 337–349. [https://doi.org/10.1016/S0034-4257\(00\)00109-7](https://doi.org/10.1016/S0034-4257(00)00109-7).
- Sun, L., Sun, C.K., Liu, Q.H., Zhong, B., 2010. Aerosol optical depth retrieval by HJ-1/CCD supported by MODIS surface reflectance data, 053. *Science China Earth Sciences*, pp. 74–80.
- Sun, L., Wei, J., Bilal, M., Tian, X., Mi, X.J.R.S., 2016. Aerosol optical depth retrieval over bright areas using Landsat 8 OLI images, 8, p. 23.
- Tang, G.Q., et al., 2016. Mixing layer height and its implications for air pollution over Beijing, China. *Atmos. Chem. Phys.* 16, 2459–2475. <https://doi.org/10.5194/acp-16-2459-2016>.
- Tanre, D., Deschamps, P.Y., Devaux, C., Herman, M., 1988. Estimation of Saharan aerosol optical thickness from blurring effects in thematic mapper data, 93. *J. Geophys. Res.-Atmos.*, pp. 15955–15964.
- Vermote, E., et al., 2006. Second Simulation of a Satellite Signal in the Solar Spectrum—Vector (6SV); 6S User Guide Version 3.
- Wang, Z.T., Li, Q., Wang, Q., Li, S., Chen, L., Zhou, C., 2012. HJ-1 terrestrial aerosol data retrieval using deep blue algorithm, 16. *Yaogan Xuebao- Journal of Remote Sensing*, pp. 596–610.
- Wei, J. et al., An improved high-spatial-resolution aerosol retrieval algorithm for MODIS images over land, (2018).
- Wei, J., et al., 2017. A simple and universal aerosol retrieval algorithm for landsat series images over complex surfaces. *J. Geophys. Res.-Atmos.* 122, 13338–13355. <https://doi.org/10.1002/2017jd026922>.
- Wei, J., Sun, L., Huang, B., Bilal, M., Environment, L.W.J.A., 2018. Verification, improvement and application of aerosol optical depths in China Part 1: inter-comparison of NPP-VIIRS and Aqua-MODIS, 175, pp. 221–233.
- Wei, J., Li, Z.Q., Peng, Y.R., Sun, L., Yan, X., 2019b. A regionally robust high-spatial-resolution aerosol retrieval algorithm for MODIS images over eastern China. *Ieee T Geosci. Rem.* 57, 4748–4757. <https://doi.org/10.1109/Tgrs.2019.2892813>.
- Wei, J., Li, Z., Peng, Y., Sun, L.J.A.E., 2019a. MODIS Collection 6.1 aerosol optical depth products over land and ocean: validation and comparison, 201, pp. 428–440.